Energy Efficient Ultrahigh Flux Separation of Oily Pollutants from Water with Superhydrophilic Nanoscale Metal–Organic Framework Architectures

Andre Mähringer, Matthias Hennemann, Timothy Clark, Thomas Bein, and Dana D. Medina*

Abstract: *The rising demand for clean water for a growing and increasingly urban global population is one of the most urgent issues of our time. Here, we introduce the synthesis of a unique nanoscale architecture of pillar-like Co-CAT-1 metal–organic framework (MOF) crystallites on gold-coated woven stainless steel meshes with large, 50 μm apertures. These nanostructured mesh surfaces feature superhydrophilic and underwater super-oleophobic wetting properties, allowing for gravity-driven, highly efficient oil–water separation featuring water fluxes of up to nearly one million $L m^{-2} h^{-1}$. Water physisorption experiments reveal the hydrophilic nature of Co-CAT-1 with a total water vapor uptake at room temperature of 470 $cm^3 g^{-1}$. Semiempirical molecular orbital calculations shed light on water affinity of the inner and outer pore surfaces. The MOF-based membranes enable high separation efficiencies for a number of liquids tested, including the notorious water pollutant, crude oil, affording chemical oxygen demand (COD) concentrations below 25 $mg L^{-1}$ of the effluent. Our results demonstrate the great impact of suitable nanoscale surface architectures as a means of encoding on-surface extreme wetting properties, yielding energy-efficient water-selective large-aperture membranes.*

Introduction

Adequate wastewater management is of great significance for a global sustainable and green economic development. By definition, wastewater is regarded as any human-affected water and can originate from a variety of diverse sources, e.g., domestic, industrial or agricultural.[1] In 2017, the United Nations released the world water development report entitled "*Wastewater, the untapped resource*" highlighting that 80% of the globally produced wastewater flows back into the ecosystem without adequate treatment or being reused.[2] Since two thirds of the world's population currently lives in areas that experience water scarcity for at least one month per year, the collection, separation, and recycling of wastewater will become a matter of vital importance.[3] One important pathway for improving water-resource management is recovering vital organic substances from waste water, enabling both to be reused after recycling processes.[2,4]

Generally, oil–water separation includes a broad range of applications such as removing oil leaks and spills, industrial wastewater treatment in oil refineries, petrochemical plants or chemical plants, or reusing wastewater for agriculture.[5] To date, several approaches for the separation of oil and water have been developed, the most prominent being the American Oil Petroleum Institute (API) oil–water separators, which are based on Stokes' law, harnessing the density difference and size of oil droplets in water for the separation.[6] Alternatively, traces of oils in water can be removed by passing the wastewater through absorber tanks containing organoclays.[7] Nowadays, membrane-based filters with nanometer pore apertures such as MOFs are emerging.[8] The separation principle of these systems is based on chemical functionalization of the membrane with hydrophobic or hydrophilic moieties.[9] By using particular functional groups, either the incoming water or oil flow is hindered according to the specific wetting properties of the membrane. A major advantage of this technique is a high separation efficiency. However, the need of applying significant backpressure to achieve sufficient flux, the chemical stability of the filter, time-consuming production, or sieving of high-profile contaminants such as crude oil are still serious challenges.[10]

In addition to employing chemical functional groups, extreme wetting properties can also be controlled through morphology.[11] According to the Wenzel or Cassie-Baxter models, rough surfaces feature enhanced wetting properties, depending on their intrinsic polarity.[12] To achieve ultrahigh flux in separations, nanowires and nanorods have been synthesized on the backbone of meshes with large apertures.[8,13] While several reports deal with oil–water separations by this approach, deterministic control over the morphology and orientation of crystalline selective layers on the mesh wires is still lacking. In addition, due to the utilization of large pore membranes the issue of water effluent quality remains largely elusive.[10]

[*] A. Mähringer, T. Bein, D. D. Medina
Department of Chemistry and Center for NanoScience (CeNS),
Ludwig-Maximilians-Universität (LMU)
Butenandtstr. 5–13, 81377 Munich (Germany)
E-mail: dana.medina@cup.lmu.de

M. Hennemann, T. Clark
Computer-Chemistry-Center, Department of Chemistry and Pharmacy, Friedrich-Alexander-University Erlangen-Nuremberg
Naegelsbachstr. 25, 91052 Erlangen (Germany)

Supporting information and the ORCID identification number(s) for the author(s) of this article can be found under:
https://doi.org/10.1002/anie.202012428.

Herein, we report highly efficient, gravity-driven and ultrahigh flux oil–water separations using an open mesh decorated with a well-defined nanoscale MOF architecture. We utilized vapor-assisted conversion (VAC) for crafting pillar-like Co-CAT-1 (Co triphenylene catecholate) MOF architectures exclusively on the mesh backbone.[14,15] Three-dimensional periodic semiempirical molecular-orbital (MO) calculations of the Co-CAT-1 water stabilization energy and water sorption experiments illustrate the high affinity of this compound towards water. According to these findings, MOF-coated mesh membrane were fabricated, several oil–water separation studies were performed. To determine the water quality after separation, the water effluent was collected, and the chemical oxygen demand (COD) concentrations were measured. Based on the COD values, we further evaluated the separation efficiencies, which ranged up to 99.98% for the MOF-based filtration system. Furthermore, we have illustrated the efficient separation of water and crude oil, driven by gravity alone, yielding cleaned water within minutes, with COD levels much below typical wastewater reuse standards.[16] The chemical and mechanical stability of the mesh were tested under different separation conditions, filtering water with acidic and basic pH and saltwater. Remarkably, the MOF-based membrane features extremely high fluxes up to nearly one million $L m^{-2} h^{-1}$, higher than a bare mesh, combined with superior water quality (COD < 25 $mg L^{-1}$).[17]

Results and Discussion

The metal–organic Co-CAT-1 framework is a microporous material consisting of the organic building block 2,3,6,7,10,11-hexahydroxytriphenylene (HHTP) connected via cobalt catecholate complex nodes forming a layered structure (Figure 1 A). A previous pioneering report elucidated the Co-CAT-1 crystal structure and the incorporation of water molecules in the crystal through complexation to the metal nodes (Figure S8).[13] This intriguing structural property
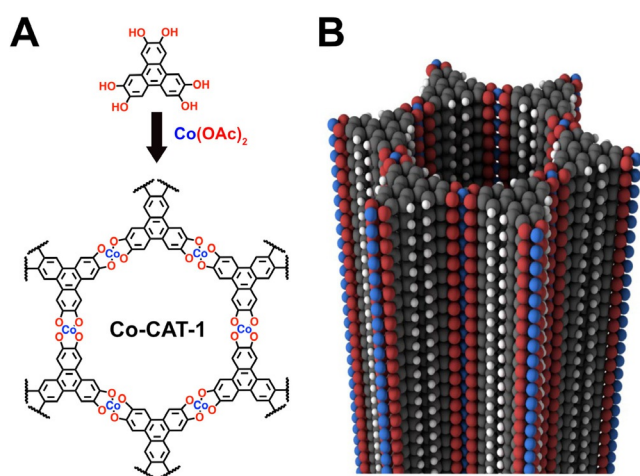
points to a highly polar pore environment, essentially increasing the effective hydrophilic surfaces. Very recently, we reported the synthesis of nanostructured and pillar-like M-CAT-1 coatings that make superhydrophilic, underwater superoleophobic and self-cleaning properties on continuous surfaces possible.[18] Thereby, the combination of well-defined and -aligned water-containing nanoporous cavities and a deterministic control of the film roughness created extreme wetting properties (Figure S9).

Here, the concept of crafting nanostructured MOF surfaces was transferred to 3D-shaped permeable objects, aimed at separating oil and water by the fundamental principle of selective flow on the basis of extreme hydrophilicity at polar surfaces. In the first part of the study, Co-CAT-1 coating was exclusively grown on the wires of stainless steel meshes (SSMs). To enable high flux and efficient oil–water separations, SSMs with large apertures of 50 μm were chosen as a preferred type of substrate (Figure 2 A). According to our previous reports, MOF materials particularly M-CAT-1 grow as crystalline and oriented thin films preferably on gold surfaces.[18] To provide gold-supported membranes, (Figure 2 B) a thin layer of 40 nm gold was deposited on the bare SSMs via physical vapor deposition (PVD) (Figure S5). A cost estimate for the gold deposition process is given in the SI. The Au@SSM obtained was used as a substrate in a VAC synthesis of Co-CAT-1 film on the mesh surface (Figure 2, S2–4). In short, a gold-coated mesh was immersed into a MOF precursor solution in a Teflon cavity holder (Figure S1). This setup was positioned on top of a glass platform in a glass autoclave. At the bottom of the autoclave, a solvent mixture bath of 1-propanol and water (5 mL; 1:1; v/v) was placed. Subsequently, the autoclave was sealed and transferred to a preheated oven at 85°C. In the course of the reaction, the solvent of the precursor solution in the small cavity was slowly evaporated, enabling a homogenous growth of the Co-CAT-1 onto the mesh wires. After 12 h, the Co-CAT-1@Au@SSM mesh was retrieved and rinsed with acetone prior to analysis.

The fabrication process of the Co-CAT-1@Au@SSMs was monitored by energy dispersive X-ray spectroscopy (EDX) mapping and back-scattered electron (BSE) microscopy (Figure S2,3). Here, continuous cobalt-containing patches exclusively covering the gold-coated parts of the mesh were observed (Figure S3). The coating is further visualized in the BSE image as a dark area (Figure 3 A) which precisely overlaps with the cobalt distribution EDX maps (Figure S2,3). Furthermore, SEM images reveal a distinct textured layer on the mesh's wires following the gold pattern, however in the proximity of the nodes where gold is absent, the MOF coating ceases. After the synthesis, the apertures of the mesh appear accessible and residual precursor or extraneous MOF material is not detected (see Figure S3). A high magnification SEM image of the Co-CAT-1@Au@SSM reveals a nanostructured surface composed of needle-like crystallites (Figure 3 B), which are preferentially aligned perpendicular to the surface (Figure S4). To confirm the formation of Co-CAT-1, the mesh surface was scratched off with a sharp razor blade and the substance obtained was transferred to a conducting copper grid for transmission electron microscopy (TEM) analysis (Figure 3 C. The electron
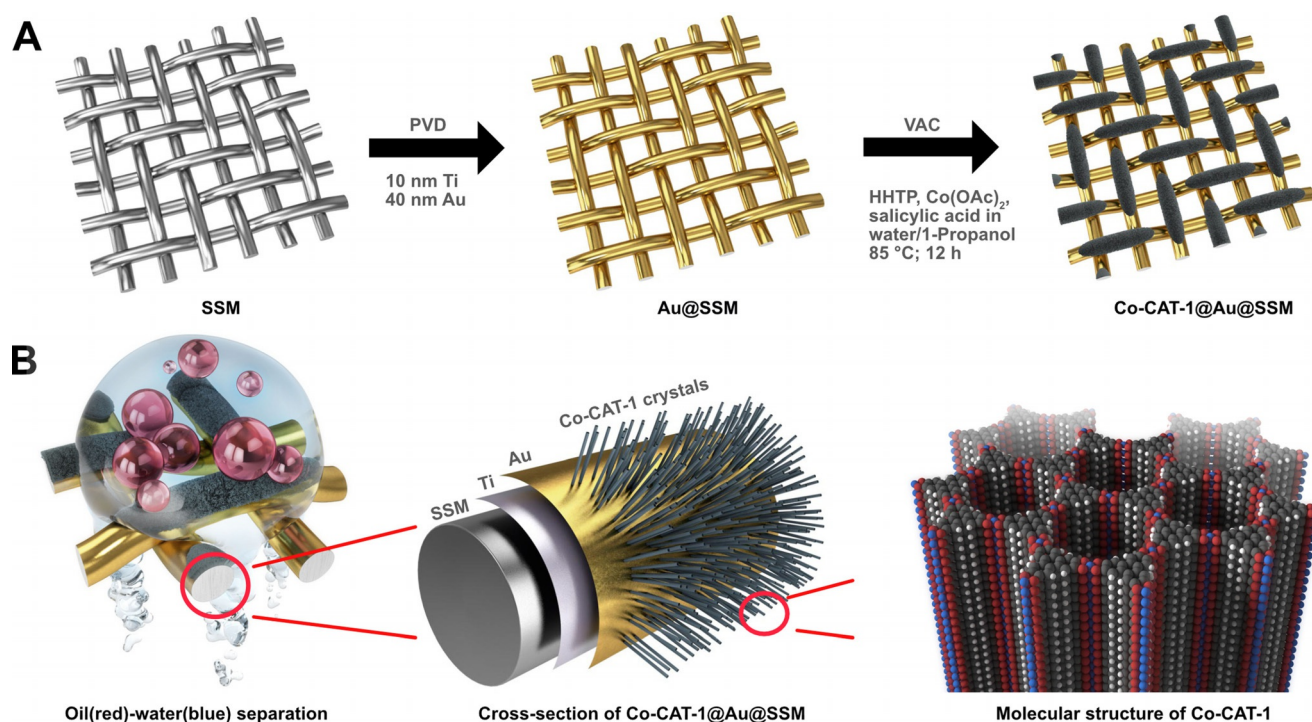

Figure 1. A) Reaction scheme of 2,3,6,7,11,12 hexahydroxytriphenylene (HHTP) and cobalt acetate tetrahydrate to form Co-CAT-1. B) The planar layers of Co-CAT-1 are stacked, forming hexagonal micropores.

Figure 2. A) A schematic illustration of the fabrication process of a MOF-based mesh. A stainless-steel mesh (SSM) with apertures of 50 μm is coated with a thin 40 nm layer of gold via physical vapor deposition (PVD). The obtained Au@SSM is used as a substrate for VAC film synthesis, resulting in the desired Co-CAT-1@Au@SSM. B) Schematic illustration of the oil–water separation by the Co-CAT-1@Au@SSM membrane blocking oil flux and allowing only water to pass through the apertures. Cross-sectional visualization of a fabricated Co-CAT-1@Au@SSM string. The Co-CAT-1 crystals consist of metal-ions in-plane coordinated by 2,3,6,7,10,11-hexahydroxytriphenylene units, forming hexagonally structured 2D layers. Finally, the MOF forms needle-like crystallites on the gold patterns encoding superhydrophilic properties on the mesh.

diffraction pattern and corresponding *d*-spacing values of the removed material are in good agreement with the calculated ones of the Co-CAT-1. Using these *d*-spacing values, the corresponding 1D diffraction pattern was calculated and the reflections were indexed according to the reported Co-CAT-1 powder X-ray diffraction (PXRD) pattern (Figure 3D, Table S1).[14] These findings confirm the formation of a highly crystalline Co-CAT-1 material on the gold-coated mesh surface. Moreover, TEM images of the scratched-off substance revealed a highly crystalline material, as indicated by the visualization of lattice fringes of the needle-like MOF crystallites and their cross-section honeycomb structure in projections along the crystal *c*-axis (Figure 3C). Notably, using higher or lower concentrations in the reaction mixture for the VAC synthesis led to uncontrolled growth of Co-CAT-1 on the mesh backbone (see Figure S6).

Next, we were intrigued to determine the wetting properties of the large pore aperture MOF-coated mesh. To assess the underwater superoleophobic properties, the underwater static oil-contact angles (OCAs) were determined for dichloromethane (DCM). Strikingly, placing a droplet of DCM on the MOF-coated open mesh surface resulted in a nearly perfect oil sphere with $OCA = 174°$ (see Figure 3E and Table S3). Static water-contact angle measurements reveal strong interactions of water with the mesh indicated by WCAs of 0° (Figure 3F). Using a high-speed camera, the time for a complete spread of the water droplet on the mesh was determined to be approximately 0.01 s (Figure 3G). These

findings confirm that the superhydrophilic and underwater superoleophobic properties can also be encoded into large pore aperture meshes through the installation of nanostructured MOF architectures exclusively on the mesh wires.

To investigate the affinity of Co-CAT-1 towards water further, we explored the water-host interactions by employing water vapor physisorption analysis and quantum chemical calculations. Using water vapor as an adsorptive at room temperature, a water vapor uptake as high as 470 cm³ g⁻¹ was measured for Co-CAT-1 powder, confirming that Co-CAT-1 is a hydrophilic material (Figure S18). Furthermore, hysteresis in the desorption curve is observed, implying strong adsorbate-adsorbate and adsorbate-adsorbent interactions. To elucidate the polar nature of the Co-CAT-1 molecular structure, calculations of the water stabilization energy inside and outside the pore were carried out. First, three-dimensional periodic AM1*[19] semiempirical molecular-orbital (MO) geometry optimizations were set up on the experimental Co-CAT-1 crystal structure reported by Yaghi and coworkers.[14] These calculations used the in-house version of EMPIRE[20] within the unrestricted Hartree–Fock (UHF) formalism using a unit cell in which all loosely bound crystal water inside the pore was omitted. Subsequently, the hydration of the pore in the optimized periodic structure was investigated using an extension of the published self-consistent reaction field (SCRF) polarizable continuum model[21] for periodic systems. These calculations gave an electrostatic water stabilization energy of -50 kcal mol⁻¹ for the inner
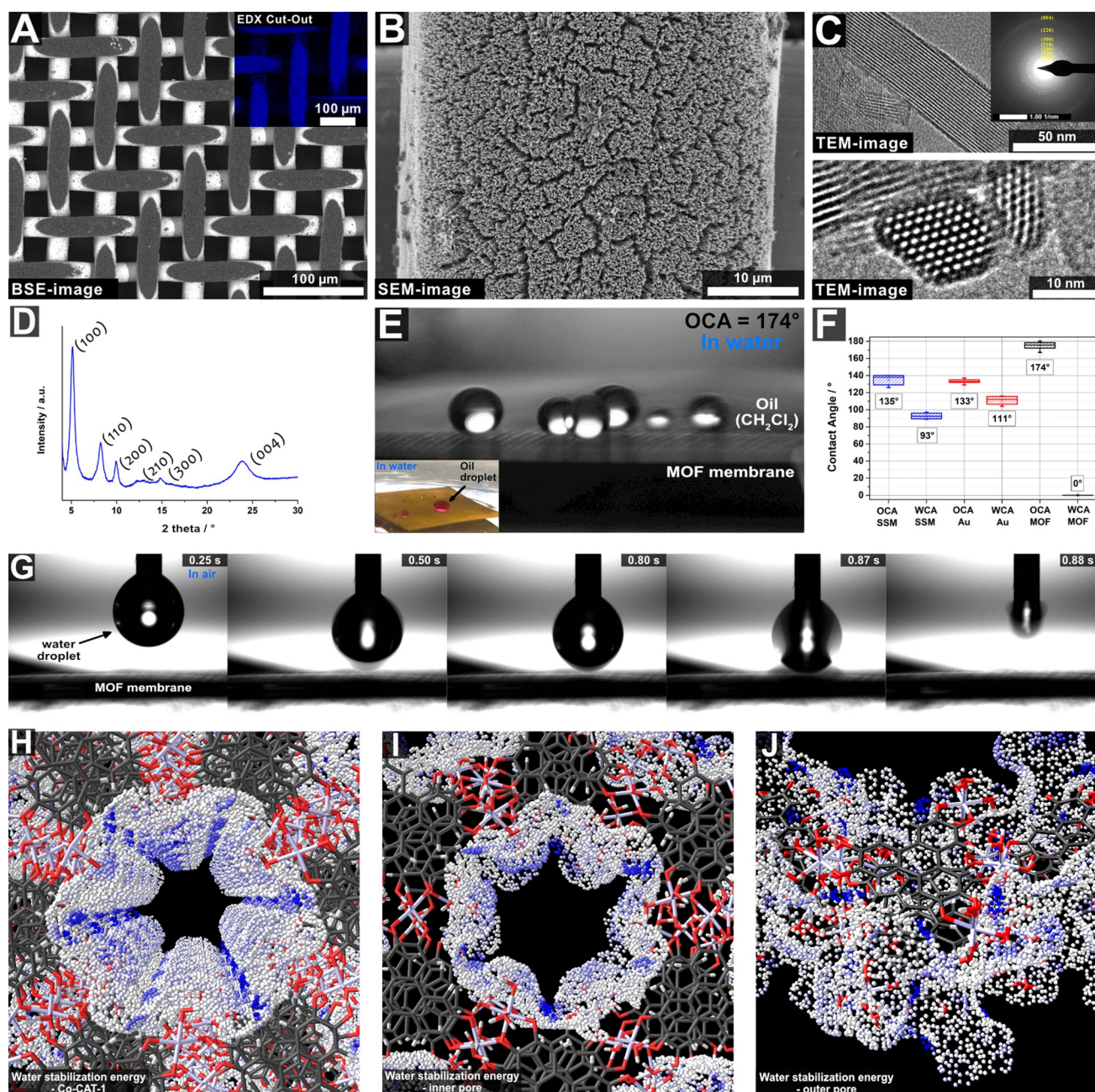
Figure 3. A) Back-scattered electron (BSE) micrograph and inset with color-coded EDX mapping of cobalt atoms (dark blue). B) High-magnification SEM image showing pillar-like crystallites. C) TEM images of the needle-shaped MOF crystallites displaying lattice fringes and the expected Co-CAT-1 honeycomb-like cross-section structure along the crystallite c-axis. D) Reconstructed 1D diffraction pattern from the TEM electron diffraction image shown as inset in C) of surface-removed MOF crystallites. E) An underwater OCA experiment using DCM as oil droplet on Co-CAT-1@Au@SSM. Inset: colored DCM oil droplets in water on the MOF-coated mesh. F) Statistics of CA for the SSM (WCA = 93°; OCA = 135°), Au@SSM (WCA = 111°; OCA = 133°), and Co-CAT-1@Au@SSM (WCA = 0°; OCA = 174°) samples. G) High-speed camera recording of the WCA of Co-CAT-1@Au@SSM showing the water droplet spread in air occurring in a time course of about 0.01 second (last two images). H) Calculation of water-pore interaction-energy surface. Color scale: Blue high interaction energy and white less interaction energy. Multiple cells along the c-direction. I) Inner and J) outer surface of the Co-CAT-1 crystallite with water-surface interaction energy.

pore and −68 kcal mol^{-1} for outer surface of the crystals per lattice cell. Both surfaces show a significant electrostatic stabilization upon hydration of the exposed surface, which agrees well with the high water uptake measured by water-vapor physisorption. Interestingly, the outer surface shows an increase of −18 kcal mol^{-1} in its absolute hydrophilic stabilization energy compared to the pore surface. These

findings are visualized in Figures 3 H–J, which show the molecular surface color coded according to the electrostatic stabilization energy for the two systems, ranging from 0.0 kcal mol^{-1} Å^{-2} (white) to −1.0 kcal mol^{-1} Å^{-2} (blue). Here, the blue areas with higher stabilizing interactions between Co-CAT-1 and water are located at the catechol-oxygen atoms of the intercalated molecular units. In contrast, at the

outer surface of the crystal additional catechol-oxygen atoms of these units are exposed, leading to a higher water affinity. These findings suggest that in these systems, the outer crystal surface area in combination with Wenzel's law plays a crucial role, enabling extreme wetting behavior.

To unlock the potential of the MOF-based mesh membrane for oil–water separations, we constructed a filtration setup based on a 3 × 3 cm large Co-CAT-1@Au@SSM mounted in a 25 mm glass microanalysis vacuum filter compartment (see Figure 4 A). Notably, the Co-CAT-1@Au@SSM filter was treated with doubly distilled water *prior* to use. Proof-of-principle oil–water separation experiments were conducted by filtering colored (Sudan-red) *n*-hexane and (methylene blue) water (Figure 4 A). For the separation, 10 mL of red-colored *n*-hexane was mixed with 10 mL of water, yielding two distinct phases. This mixture was poured into a glass column and subsequently onto the MOF-based membrane (Figure S12). Remarkably, water easily flowed and passed the filter while the red-colored *n*-hexane liquid was blocked on the filter opening, resulting in a standing red oil column. Furthermore, adding an additional 30 mL of water to the oil-containing glass tube resulted in water percolation through the red-colored oil. The water easily passed through the MOF-based filter membrane and was subsequently collected in the collecting vessel, while the oil column remained intact. To the naked eye, the filtered water was clear and red-colored oil residue contaminants were not visible. To target a wide range of water contaminants, the MOF-based membrane was subjected to different oil–water compositions where the separation efficiencies, residual oil-content in the water effluent and the water flux were determined (for further information see Materials and Methods). Hereby, lightweight oils such as *n*-hexane and *n*-pentane, 1-dodecene (as an example for diesel fuel resembling the general sum formula $C_{12}H_{24}$)[22] and paraffin oils such as polydimethylsiloxane, cycloalkanes, aromatic hydrocarbons, economically relevant oils such as xylene (mixture of *ortho*-, *meta*-, and *para*-isomers) and crude oil were investigated. The water quality after filtration of the different oil–water mixtures was determined by chemical oxygen demand (COD) measurements. This indirect measurement is widely used for the quantitative detection of organic residuals in waste and drinking water and is an important indicator of water quality.[16] The COD value is displayed as the equivalent amount of oxygen required for the oxidation of the organic pollutant in one liter of the analyzed water (for further information about the COD analysis see the SI). For evaluating the resulting water quality, a liquid mixture (3:1; v:v; 150 mL) of water and oil was filtered with the MOF-based membrane as shown exemplarily in Figure S12. After filtration, the effluent was collected, and its COD was determined. For each of the oil-contaminated water samples, water was collected from five filtration batches and subsequently subjected to the COD test (Figure 4 B and Table S4).

Notably, all the tested water samples exhibit low COD values ranging from 0.6 mg L^{-1} to 24.3 mg L^{-1} (averaged values after 5 cycles). To put these results in perspective, the COD values of tap water and surface water samples are in the
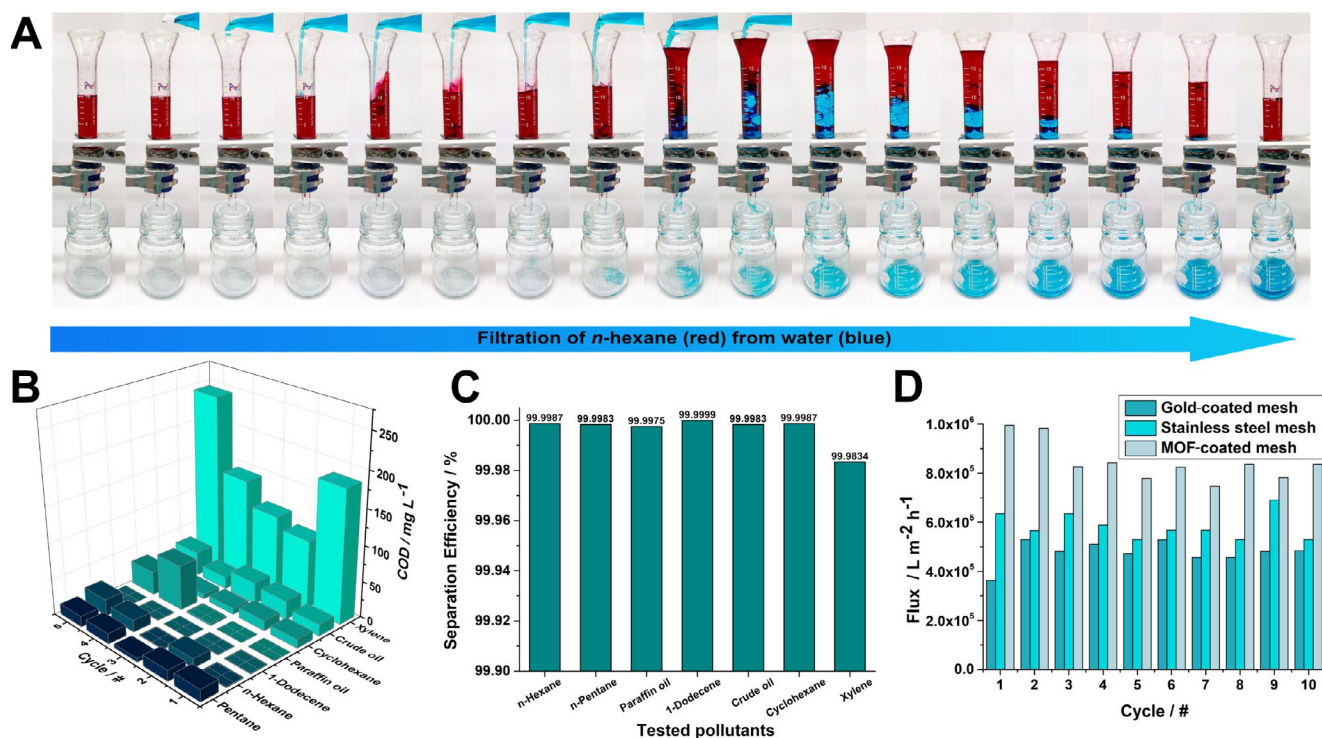

Figure 4. A) Image sequence illustrating the course of filtration of water through the MOF-based filter setup. As oily liquid, colored (sudan-red) *n*-hexane was used. B) 3D bar diagram of the measured COD values for the filtrated water samples. C) Water and oil separation efficiencies of *n*-pentane, *n*-hexane, 1-dodecene, paraffin oil, cyclohexane, xylene and crude oil. D) Measured water flux through SSM (cyan) Au@SSM (turquois), and Co-CAT-1@Au@SSM (light cyan) filter systems. The experimental work shown in Figure 3 is supported by further statistical data (see Figures S13–15).

range of 20 mg L^{-1}.[23] These findings confirm that the MOF-based membrane filtration system is suitable for the high-quality separation of a wide range of oily liquids from water. Importantly, water and industrially relevant substances such as 1-dodecene are separated most efficiently by the MOF-based filtration system. So far, we had investigated the separation of poorly soluble oils in the water phase. We therefore analyzed a xylene-water mixture as a model for an oily contaminant featuring increased solubility in water. For comparison, the solubility of xylene in water is 20 times greater than that of *n*-hexane. Here, slightly higher average COD concentrations of 155.3 mg L^{-1} were determined for the water effluent (corresponding to a xylene conc. of 48.9 mg L^{-1}). It is important to emphasize that the COD value requirements for safe wastewater disposal for the chemical industry in Germany lie between 75 mg L^{-1} and 2500 mg L^{-1}; the specific COD value depends on the pollutant concentrations at the site of occurrence in the industrial process.[16] In this work, the large majority of the tested water samples after one single cycle of filtration were well below this limit and would be suitable for disposal without further treatment. Even in the case of more water-soluble contaminants such as xylene isomers, the COD concentrations are still within the safe range for wastewater disposal (Figure 4B).

The oil–water separation efficiency was determined by calculating the molar amount of pollutant in water before and after filtration (Figure 4C). Assuming a stoichiometric reaction of oxygen and the organic pollutant and using the COD values afforded the molar amount of organic pollutant per liter of water. To obtain the separation efficiencies, this value was placed in relation to oil fraction amount before filtration of the oil–water mixture. For the different oil–water mixtures, separation-efficiency values of up to 99.99 % were calculated. Water-xylene isomers gave slightly lower efficiencies of 99.98 % due to the greater solubility of the aromatic compound in water (see Table S5). Control experiments for the SSM and Au@SSM are shown in Figures S10–11.

The gravity-driven water flux measurements were conducted by allowing a 10 cm high water column to run through the Co-CAT-1@Au@SSM until completion (for further details see SI). The water flux through the MOF-coated mesh was compared to that of the analogous SSM and Au@SSM filters (Figure 4D). Hereby, the exceptionally high average water flux increased in the order Au@SSM (3.8×10^5 L h^{-1} m^{-2}) < SSM (6.2×10^5 L h^{-1} m^{-2}) < Co-CAT-1@Au@SSM (8.4×10^5 L h^{-1} m^{-2}). These flux values are conservative estimates due to the progressing reduction of water column height during the process. Nevertheless, to the best of our knowledge the Co-CAT-1@Au@SSM offers the highest flux reported for MOF-modified open meshes[17] (for further information see Tables S6–8). The results illustrate that the MOF nanostructure even enhances the water flux (by a factor of ca. 1.3) through the membrane compared to the bare stainless steel mesh, while adding the important property of oil blocking. We attribute this notable increase of the flux to the superhydrophilic nature of the nanostructured MOF, which leads to a complete wetting of the surface of the mesh with water, thereby reducing the forces acting on the mesh during the flow, similar to natural phenomena observed, for example, at the surface of shark skin.[24]

To illustrate the impact of filtration based purely on surface wetting and gravity further, we focused on the separation of water and crude oil (Figure 5). Crude oil is responsible for severe environmental damage and catastrophic oil leaks or spills on the open sea or in rivers. It consists of different alkanes, cycloalkanes and various aromatic hydrocarbons containing different traces of metals, bacteria and sulfur. It typically forms a dark viscous suspension, which is very challenging to extract or to separate from water. Using the MOF-based filtration system, the separation of water and a crude oil pollutant mixture was demonstrated, yielding an apparently clear and clean extract (Figure 5D). Remarkably, the measured COD value for the collected water was determined to be as low as 24.3 mg L^{-1} (average value after five filtration cycles; see Table S4), making the filtered water ready for disposal as harmless wastewater without further cleanup.

The integrity of the MOF filter system is of paramount importance for filtration of water from industrial processes or emerging from natural sources. Therefore, we verified the stability of the MOF-membrane by measuring the OCA and WCA after every fifth cycle of a total of 25 filtration cycles in
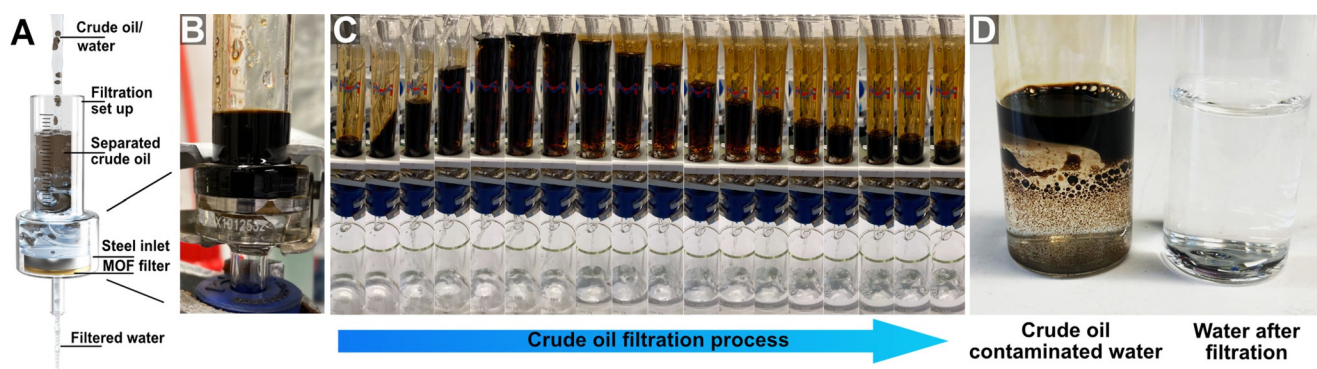

Figure 5. A) Experimental setup for the separation of crude oil from doubly-distilled (dd) water. B) Magnified depiction of the crude oil and MOF filter interface in the separation set up. C) Image series monitoring the separation of water from crude oil. D) Image showing the qualitative result of the separation. Left side depicts the crude oil contaminated water sample before filtration. Right side illustrates the same water after filtration with the Co-CAT-1@Au@SSM filter setup. The measured average COD value is below 25 mg L^{-1}.

doubly distilled (dd) water as reference, saltwater (exemplary for sea water, 3.5 wt. % NaCl) and water of pH 6 and 8 (see Table S10 and Figures S16,17). Here, the extreme wetting properties of the membrane were maintained throughout these filtration cycles. (Figure S17). Furthermore, 25 liters of water were filtered in total through the MOF-based filter in a total of 50 filtration iterations. Subsequently, effluent samples were collected after every fifth cycle and tested using inductively coupled plasma atomic emission spectrometry (ICP-AES; limit of detection $= 10 \, ng \, mL^{-1}$, Table S11). Importantly, no traces of cobalt ions were detected in the effluents. These findings suggest that the MOF film is stable during the filtration process and that no harmful metal ions are released from the filter to the collected water. Furthermore, the breakthrough time of a 10 cm oil column (150 mL n-hexane) on a 7 mm^2 sized Co-CAT-1@Au@SSM filter fused to the bottom (1.5 cm in diameter) of a polyester vessel was found to be ca. 6 h (see Figure S16). After breakthrough, the underwater superoleophobic behavior can be recovered by simple re-wetting of the Co-CAT-1@Au@SSM filter with dd-water.

Conclusion

Summarizing, the combination of a specifically designed nanoscale architecture with aligned and accessible polar nanocavities in MOF crystal needles endows a stainless steel membrane with outstanding, wetting capabilities. The super-hydrophilic nature of Co-CAT-1 crystallites was elucidated by water vapor physisorption measurements and quantum mechanical modeling, confirming the high affinity of the molecular structure towards water. Subsequently, a proof-of-principle water filtration setup was constructed using 3×3 cm large MOF-functionalized meshes. With this setup, several oily fluids including the notorious water pollutant crude oil were successfully separated from water. The key point is that the aqueous phase freely passes the superhydrophilic mesh with only gravity as the driving force, while the flow of the hydrophobic oily phase is completely blocked. Oil–water separation efficiencies were measured by calculating the concentration of pollutant before and after filtration in one liter of water. For the oily substances tested, efficiencies of 99.99–99.98 % were reached. Importantly, low COD values ranging from 0.64 mg L^{-1} to 24.3 mg L^{-1} were determined for the filtered water effluents, depending on the nature of the oily phase. Therefore, the water quality obtained after filtration is in every tested case high (close to tap water quality) and can therefore be reused for different purposes.[16,25] These outstanding filtration abilities are based purely on highly unusual wetting properties induced by the nanoscale MOF architecture on the mesh. Moreover, the accessible 50 μm mesh apertures allow for extremely high water flux reaching nearly one million L h^{-1} m^{-2}, driven simply by gravity, which eliminates the need for applying backpressure. Therefore, these MOF-based filters are highly suitable for applications where a high water flux and low driving force are needed, such as large-scale separations or water purification in remote areas without the need for any moving parts. The stability of the MOF-based filters was verified at different pH values and environmental factors such as salt-water. These findings show that the MOF-modified meshes can operate even under substantially different and challenging conditions. Furthermore, the chemical integrity of the MOF coating was studied by ICP-AES, showing no traces of cobalt ions in the filtered water after filtration of 25 liters of water. Finally, we note that this MOF-based separation system can serve as a structural blueprint for additional nanoscale porous architectures suitable for morphology-based separations. Thereby, other features of interest such as rapid production methods, desirable mechanical properties or stability against fouling could be engineered into the open mesh system while maintaining the highly efficient separation capabilities.

Acknowledgements

Conflict of interest

The authors declare no conflict of interest.

[1] T. Asano, *Water reuse. Issues, technology, and applications*, McGraw-Hill, New York, NY, **2007**.

[2] *Wastewater. The untapped resource*, UNESCO, Paris, **2017**.

[3] H. Kim, S. R. Rao, E. A. Kapustin, L. Zhao, S. Yang, O. M. Yaghi, E. N. Wang, *Nat. Commun.* **2018**, *9*, 1191.

[4] a) S. Sengupta, T. Nawaz, J. Beaudry, *Curr. Pollut. Rep.* **2015**, *1*, 155; b) A. Alsbaiee, B. J. Smith, L. Xiao, Y. Ling, D. E. Helbling, W. R. Dichtel, *Nature* **2016**, *529*, 190.

[5] a) E. Ankyu, R. Noguchi, *Procedia. Agric. Ecosyst. Environ.* **2014**, *2*, 67; b) S. Munirasu, M. A. Haija, F. Banat, *Process Saf. Environ.* **2016**, *100*, 183; c) A. Fakhru'l-Razi, A. Pendashteh, L. C. Abdullah, D. R. A. Biak, S. S. Madaeni, Z. Z. Abidin, *J. Hazard.* **2009**, *170*, 530; d) M. Sarcletti, D. Vivod, T. Luchs, T. Rejek, L. Portilla, L. Müller, H. Dietrich, A. Hirsch, D. Zahn, M. Halik, *Adv. Funct. Mater.* **2019**, *29*, 1805742.

[6] American Petroleum Institute., Division of Refining., *Design and operation of oil–water separators*, American Petroleum Institute, Washington, D. C., **1990**.

[7] G. R. Alther, *Water Eng. Manage.* **2001**, *148*, 27.

[8] R. K. Gupta, G. J. Dunderdale, M. W. England, A. Hozumi, *J. Mater. Chem. A* **2017**, *5*, 16025.

[9] a) L. Feng, Z. Zhang, Z. Mai, Y. Ma, B. Liu, L. Jiang, D. Zhu, *Angew. Chem. Int. Ed.* **2004**, *43*, 2012; *Angew. Chem.* **2004**, *116*,

2046; b) G. J. Dunderdale, M. W. England, T. Sato, C. Urata, A. Hozumi, *Macromol. Mater. Eng.* **2016**, *301*, 1032; c) J. G. Nguyen, S. M. Cohen, *J. Am. Chem. Soc.* **2010**, *132*, 4560; d) K. He, H. Duan, G. Y. Chen, X. Liu, W. Yang, D. Wang, *ACS Nano* **2015**, *9*, 9188; e) K. P. Rao, M. Higuchi, K. Sumida, S. Furukawa, J. Duan, S. Kitagawa, *Angew. Chem. Int. Ed.* **2014**, *53*, 8225; *Angew. Chem.* **2014**, *126*, 8364; f) K. Jayaramulu, K. K. R. Datta, C. Rösler, M. Petr, M. Otyepka, R. Zboril, R. A. Fischer, *Angew. Chem. Int. Ed.* **2016**, *55*, 1178; *Angew. Chem.* **2016**, *128*, 1193.

[10] B. Wang, W. Liang, Z. Guo, W. Liu, *Chem. Soc. Rev.* **2015**, *44*, 336.

[11] a) R. N. Wenzel, *Ind. Eng. Chem.* **1936**, *28*, 988; b) A. B. D. Cassie, S. Baxter, *Trans. Faraday Soc.* **1944**, *40*, 546; M. Liu, S. Wang, L. Jiang, *Nat. Rev. Mater.* **2017**, *2*, 17036.

[12] a) J. Yong, F. Chen, Q. Yang, J. Huo, X. Hou, *Chem. Soc. Rev.* **2017**, *46*, 4168; b) L. Wen, Y. Tian, L. Jiang, *Angew. Chem. Int. Ed.* **2015**, *54*, 3387; *Angew. Chem.* **2015**, *127*, 3448; c) S. Wang, K. Liu, X. Yao, L. Jiang, *Chem. Rev.* **2015**, *115*, 8230.

[13] a) F. Zhang, W. B. Zhang, Z. Shi, D. Wang, J. Jin, L. Jiang, *Adv. Mater.* **2013**, *25*, 419; b) Q. Wen, J. Di, L. Jiang, J. Yu, R. Xu, *Chem. Sci.* **2013**, *4*, 591; c) J. Zeng, Z. Guo, *Colloids Surf. A* **2014**, *444*, 283; d) Q. Ma, P. Yin, M. Zhao, Z. Luo, Y. Huang, Q. He, Y. Yu, Z. Liu, Z. Hu, B. Chen, et al., *Adv. Mater.* **2019**, *31*, 1808249.

[14] M. Hmadeh, Z. Lu, Z. Liu, F. Gándara, H. Furukawa, S. Wan, V. Augustyn, R. Chang, L. Liao, F. Zhou, et al., *Chem. Mater.* **2012**, *24*, 3511.

[15] a) V. Rubio-Giménez, M. Galbiati, J. Castells-Gil, N. Almora-Barrios, J. Navarro-Sánchez, G. Escorcia-Ariza, M. Mattera, T. Arnold, J. Rawle, S. Tatay, et al., *Adv. Mater.* **2018**, *30*, 1704291; b) M. K. Smith, K. E. Jensen, P. A. Pivak, K. A. Mirica, *Chem. Mater.* **2016**, *28*, 5264.

[16] Federal Environmental Ministry of Germany Federal Law Gazette BGBl. I p. 1108.

[17] X. Zhang, H. Li, W. Miao, Q. Shen, J. Wang, D. Peng, J. Liu, Y. Zhang, *AIChE J.* **2019**, *65*, e16596.

[18] a) A. Mähringer, J. M. Rotter, D. D. Medina, *Beilstein J. Nanotechnol.* **2019**, *10*, 1994; b) A. Mähringer, A. C. Jakowetz, J. M. Rotter, B. J. Bohn, J. K. Stolarczyk, J. Feldmann, T. Bein, D. D. Medina, *ACS Nano*, **2019**, *13*, 6711; c) E. Virmani, J. M. Rotter, A. Mähringer, T. Zons, A. Godt, T. Bein, S. Wuttke, D. D. Medina, *J. Am. Chem. Soc.*, **2018**, *140*, 4812.

[19] a) M. J. S. Dewar, E. G. Zoebisch, E. F. Healy, J. J. P. Stewart, *J. Am. Chem. Soc.* **1985**, *107*, 3902–3909; b) P. Winget, A. H. C. Horn, C. Selçuki, B. Martin, T. Clark, *J. Mol. Model.* **2003**, *9*, 408–414; c) H. Kayi, T. Clark, *J. Mol. Model.* **2010**, *16*, 29–47.

[20] a) M. Hennemann, T. Clark, *J. Mol. Model.* **2014**, *20*, 2331; b) J. T. Margraf, M. Hennemann, B. Meyer, T. Clark, *J. Mol. Model.* **2015**, *21*, 144.

[21] G. Rauhut, T. Clark, T. Steinke, *J. Am. Chem. Soc.* **1993**, *115*, 9174–9181.

[22] C. Soares in *Gas turbines. A handbook of air, land and sea applications* (Ed.: C. Soares), Butterworth-Heinemann is an imprint of Elsevier, Kidlington, **2015**, pp. 317–411.

[23] D. Chapman, *Water Quality Assessments*, Taylor & Francis, Abingdon, UK, **1992**.

[24] G. D. Bixler, B. Bhushan, *Nanoscale* **2013**, *5*, 7685.

[25] W. H. Organization, *Guidelines for Drinking-water Quality*, World Health Organization, Geneva, **2011**.